

Search for the decay $B_s^0 \rightarrow \bar{D}^0 f_0(980)$



The LHCb collaboration

E-mail: mwhitehe@cern.ch

ABSTRACT: A search for $B_s^0 \rightarrow \bar{D}^0 f_0(980)$ decays is performed using 3.0 fb^{-1} of pp collision data recorded by the LHCb experiment during 2011 and 2012. The $f_0(980)$ meson is reconstructed through its decay to the $\pi^+\pi^-$ final state in the mass window $900 \text{ MeV}/c^2 < m(\pi^+\pi^-) < 1080 \text{ MeV}/c^2$. No significant signal is observed. The first upper limits on the branching fraction of $\mathcal{B}(B_s^0 \rightarrow \bar{D}^0 f_0(980)) < 3.1 (3.4) \times 10^{-6}$ are set at 90% (95%) confidence level.

KEYWORDS: Hadron-Hadron Scattering, Branching fraction, B physics, Flavor physics

ARXIV EPRINT: [1505.01654](https://arxiv.org/abs/1505.01654)

Contents

1	Introduction	1
2	LHCb detector	2
3	Selection	3
4	Determination of signal yield	4
5	Systematic uncertainties	5
6	Results and summary	8
	The LHCb collaboration	14

1 Introduction

Understanding the quark-level substructure of the scalar mesons is one of the main challenges in hadronic physics. The number of observed states, and their masses and branching fractions, suggest that there is a contribution from four-quark wavefunctions in addition to $q\bar{q}$, and possible gluonic, degrees of freedom [1, 2]. However, the extent of mixing between the different components is unclear.

Measurement of the relative production of scalar mesons in B^0 and B_s^0 meson decays can help to address this issue [3, 4]. Measurements of $B_{(s)}^0 \rightarrow J/\psi f$ decays, where f represents either the $f_0(500)$ (also known as σ) or the $f_0(980)$ meson, and $f \rightarrow \pi^+\pi^-$ [5–8] have already provided important insight into the structure of the scalar mesons [9, 10]. Studies of $B_{(s)}^0 \rightarrow \bar{D}^0 f$ decays provide complementary information to the $B_{(s)}^0 \rightarrow J/\psi f$ case [11]. Measurements of the branching fractions of $B^0 \rightarrow \bar{D}^0 f_0(500)$ and $B^0 \rightarrow \bar{D}^0 f_0(980)$ decays have been obtained from Dalitz plot analyses of $B^0 \rightarrow \bar{D}^0 \pi^+ \pi^-$ decays [12, 13], but there is no experimental result to date on the B_s^0 decays.

In addition, under the assumption that the $f_0(980)$ meson has a predominant $s\bar{s}$ component, the $B_s^0 \rightarrow \bar{D}^0 f_0(980)$ decay mode can be used to determine the angle γ of the CKM unitarity triangle [14, 15], using the same methods that are applicable for the $B_s^0 \rightarrow \bar{D}^0 \phi$ decay mode [16–20]. Since the $B_s^0 \rightarrow \bar{D}^0 \phi$ decay has recently been observed [21], a signal for the $B_s^0 \rightarrow \bar{D}^0 f_0(980)$ channel is expected if the branching fractions of the two decays are comparable. An explicit calculation predicts $\mathcal{B}(B_s^0 \rightarrow \bar{D}^0 f_0(980)) = (3.50_{-1.15}^{+1.26} {}_{-0.77}^{+0.56}) \times 10^{-5}$ [22].

In this paper, the result of a search for the $B_s^0 \rightarrow \bar{D}^0 f_0(980)$ decay is presented. The inclusion of charge conjugated processes is implied throughout the paper. The final state

is reconstructed through the $\bar{D}^0 \rightarrow K^+\pi^-$ and $f_0(980) \rightarrow \pi^+\pi^-$ decays. The decay-time-integrated branching fraction is measured under the assumption that the $B_s^0 \rightarrow \bar{D}^0\pi^+\pi^-$ decay proceeds uniquely via the $f_0(980)$ resonance within the selected mass window, $900 \text{ MeV}/c^2 < m(\pi^+\pi^-) < 1080 \text{ MeV}/c^2$. This approach was used for the first observation of $B_s^0 \rightarrow J/\psi f_0(980)$ decays [23]; it is also justified by the fact that no other contribution to $B_s^0 \rightarrow \bar{D}^0\pi^+\pi^-$ decays, for example through the $B_s^0 \rightarrow D^{*-}\pi^+$ process [24], is expected at the current level of sensitivity. A further assumption is that the contribution from $B_s^0 \rightarrow D^0 f_0(980)$ decays, which is suppressed by the ratio of CKM matrix elements $|V_{ub}V_{cs}^*/(V_{cb}V_{us}^*)|^2 \approx 0.1$, is negligible. Formally, the measurement is of the decay-time-integrated sum of the branching fractions for $B_s^0 \rightarrow \bar{D}^0 f_0(980)$ and $B_s^0 \rightarrow D^0 f_0(980)$ decays.

The analysis is based on 3.0 fb^{-1} of LHC pp collision data collected with the LHCb detector, with approximately one third taken at a centre-of-mass energy of 7 TeV during 2011 and the remainder at 8 TeV during 2012. The measurement is obtained by evaluating the ratio of branching fractions

$$\frac{\mathcal{B}(B_s^0 \rightarrow \bar{D}^0 f_0(980))}{\mathcal{B}(B^0 \rightarrow \bar{D}^0 \pi^+ \pi^-)} = \frac{N(B_s^0 \rightarrow \bar{D}^0 f_0(980))}{N(B^0 \rightarrow \bar{D}^0 \pi^+ \pi^-)} \times \frac{\epsilon(B^0 \rightarrow \bar{D}^0 \pi^+ \pi^-)}{\epsilon(B_s^0 \rightarrow \bar{D}^0 f_0(980))} \times \frac{f_d}{f_s}, \quad (1.1)$$

from which the absolute branching fraction for $B_s^0 \rightarrow \bar{D}^0 f_0(980)$ decays is determined using the known value of $\mathcal{B}(B^0 \rightarrow \bar{D}^0 \pi^+ \pi^-)$ [13]. The yields $N(B_s^0 \rightarrow \bar{D}^0 f_0(980))$ and $N(B^0 \rightarrow \bar{D}^0 \pi^+ \pi^-)$ are determined from separate extended maximum likelihood fits to the distributions of selected $\bar{D}^0 f_0(980)$ and $\bar{D}^0 \pi^+ \pi^-$ candidates in both the B candidate mass and the output of a neural network (NN) used to separate signal from combinatorial background. The combined reconstruction and selection efficiencies, $\epsilon(B_s^0 \rightarrow \bar{D}^0 f_0(980))$ and $\epsilon(B^0 \rightarrow \bar{D}^0 \pi^+ \pi^-)$, are determined from simulated samples with data-driven corrections applied. The ratio of fragmentation fractions inside the LHCb acceptance has been measured to be $f_s/f_d = 0.259 \pm 0.015$ ([25], f_s/f_d value updated in [26]). Equation (1.1) corresponds to a branching fraction for $f_0(980) \rightarrow \pi^+\pi^-$ of 100%, which is the conventional way to quote results for decays involving $f_0(980)$ mesons.

2 LHCb detector

The LHCb detector [27, 28] is a single-arm forward spectrometer covering the pseudorapidity range $2 < \eta < 5$, designed for the study of particles containing b or c quarks. The detector includes a high-precision tracking system consisting of a silicon-strip vertex detector [29] surrounding the pp interaction region, a large-area silicon-strip detector located upstream of a dipole magnet with a bending power of about 4 Tm, and three stations of silicon-strip detectors and straw drift tubes [30] placed downstream of the magnet. The tracking system provides a measurement of momentum, p , of charged particles with a relative uncertainty that varies from 0.5% at low momentum to 1.0% at 200 GeV/ c . The minimum distance of a track to a primary vertex, the impact parameter (IP), is measured with a resolution of $(15 + 29/p_T) \mu\text{m}$, where p_T is the component of the momentum transverse to the beam, in GeV/ c . Different types of charged hadrons are distinguished

using information from two ring-imaging Cherenkov detectors [31]. Photon, electron and hadron candidates are identified by a calorimeter system consisting of scintillating-pad and preshower detectors, an electromagnetic calorimeter and a hadronic calorimeter. Muons are identified by a system composed of alternating layers of iron and multiwire proportional chambers [32].

The trigger [33] consists of a hardware stage, based on information from the calorimeter and muon systems, followed by a software stage, in which all tracks with $p_T > 500$ (300) MeV are reconstructed for 2011 (2012) data. The software trigger requires a two-, three- or four-track secondary vertex with significant displacement from the primary pp interaction vertices (PVs). At least one charged particle must have $p_T > 1.7$ GeV/ c and be inconsistent with originating from a PV. A multivariate algorithm [34] is used for the identification of secondary vertices consistent with the decay of a b hadron.

Simulated events are used to characterise the detector response to signal and certain types of background events. In the simulation, pp collisions are generated using PYTHIA [35, 36] with a specific LHCb configuration [37]. Decays of hadronic particles are described by EVTGEN [38], in which final state radiation is generated using PHOTOS [39]. The interaction of the generated particles with the detector and its response are implemented using the GEANT4 toolkit [40, 41] as described in ref. [42].

3 Selection

Candidates consistent with the decay chain $B_{(s)}^0 \rightarrow \bar{D}^0 \pi^+ \pi^-$ with $\bar{D}^0 \rightarrow K^+ \pi^-$ are selected. The selection procedure involves applying a preselection to the data sample before using a NN to reduce the combinatorial background. The NN [43] is trained with the pre-selected $\bar{D}^0 \pi^+ \pi^-$ data sample, using the *sPlot* method [44] with the B candidate mass as discriminating variable to separate statistically the signal and background categories. The input variables to the NN are related to the kinematic properties of the candidate, its isolation from the rest of the pp collision event, and the topology of the signal decay chain. Full details of the preselection and NN training can be found in ref. [45]. The four final-state tracks must also satisfy particle identification (PID) requirements. Signal candidates are retained for further analysis if they have invariant mass in the range 5100–5900 MeV/ c^2 . A requirement that the NN output is greater than -0.7 removes 77% of combinatorial background and retains 95% of $B_s^0 \rightarrow \bar{D}^0 f_0(980)$ decays.

A requirement $m(\bar{D}^0 \pi^-) > 2.10$ GeV/ c^2 is used to remove candidates that predominantly originate from $B^0 \rightarrow D^{*-} \pi^+$ decays. A further requirement, $m(\bar{D}^0 \pi^+) < 5.14$ GeV/ c^2 , is used to remove backgrounds from $B^+ \rightarrow \bar{D}^0 \pi^+$ decays combined with a random π^- candidate. This source of combinatorial background is kinematically excluded from the signal region, but causes structure in the mass distribution at higher B candidate mass. A similar contribution from $B^+ \rightarrow \bar{D}^{*0} \pi^+$ decays cannot be vetoed in the same way, and must therefore be considered further as a source of background.

Following all selection requirements, approximately 1% of events contain more than one candidate. All candidates are retained for the subsequent analysis; the associated systematic uncertainty is negligible.

4 Determination of signal yield

The yields of $B_s^0 \rightarrow \bar{D}^0 f_0(980)$ and $B^0 \rightarrow \bar{D}^0 \pi^+ \pi^-$ decays are obtained from two separate extended maximum likelihood fits to the distributions of NN output and B candidate mass for selected candidates. The only difference between the samples used in the two fits is that the former has an additional requirement of $900 \text{ MeV}/c^2 < m(\pi^+ \pi^-) < 1080 \text{ MeV}/c^2$. The yield of $B_s^0 \rightarrow \bar{D}^0 \pi^+ \pi^-$ decays in the latter fit is expected to be negligible compared to the large yields of B^0 decays and combinatorial background, and is therefore fixed to zero. However, a significant number of $B^0 \rightarrow \bar{D}^0 \pi^+ \pi^-$ decays are expected to remain within the $f_0(980)$ mass window [13], and therefore both B^0 and B_s^0 components are included in the former fit.

The data are divided into five bins of the NN output variable, defined as $[-0.70, 0.03]$, $[0.03, 0.54]$, $[0.54, 0.77]$, $[0.77, 0.88]$ and $[0.88, 1.00]$, and referred to hereafter as bins 1 to 5, respectively. The five bins contain a similar proportion of signal decays and increase in purity from bin 1 to bin 5. This choice of binning has been found to enhance the sensitivity whilst giving stable fit performance.

The fits include components due to signal and combinatorial background as well as from partially reconstructed and misidentified b -hadron decays. The signal invariant mass distribution is described by the sum of two Crystal Ball (CB) [46] functions, with a shared mean and tails on opposite sides described by parameters that are fixed to values found in fits to simulated samples.

The combinatorial background is modelled with the sum of two components. The first has an exponential shape, described by a parameter that is the same in all NN bins. The second originates from $B^+ \rightarrow \bar{D}^{*0} \pi^+$ decays combined with a random pion candidate, and is modelled using a non-parametric shape determined from simulation. The limited sizes of the simulated samples used to obtain this and similar shapes are sources of systematic uncertainty.

Partially reconstructed backgrounds occur from $B^0 \rightarrow \bar{D}^{*0} \pi^+ \pi^-$ decays, with $\bar{D}^{*0} \rightarrow \bar{D}^0 \pi^0$ and $\bar{D}^{*0} \rightarrow \bar{D}^0 \gamma$ where the neutral pion or photon is not associated with the candidate, and from $B^+ \rightarrow \bar{D}^0 \pi^+ \pi^- \pi^+$ decays where one π^+ is also not associated with the candidate. The invariant mass shapes of these backgrounds are described with non-parametric functions derived from simulation. A global offset of the shape of the partially reconstructed background is determined from the fit to data to allow for differences between data and simulation [47].

Backgrounds from misidentified b -hadron decays arise from $B^0 \rightarrow \bar{D}^{(*)0} K^+ \pi^-$ and $B_s^0 \rightarrow \bar{D}^{(*)0} K^- \pi^+$ (hereafter collectively referred to as $B_{(s)}^0 \rightarrow \bar{D}^{(*)0} K \pi$) decays where the kaon is misidentified as a pion and from $\Lambda_b^0 \rightarrow D^{(*)0} p \pi^-$ decays where the proton is misidentified as a pion. Simulation is used to obtain non-parametric descriptions of the invariant mass shapes. To obtain these shapes, the latest knowledge of the phase-space distributions of the decays [45, 48, 49], of the relative branching fractions of the B^0 and $B_s^0 \rightarrow \bar{D}^0 K \pi$ modes [48], and of the relative branching fractions of the decays involving \bar{D}^0 and \bar{D}^{*0} mesons [2], is used. Data-driven estimates of the misidentification probability as a function of particle kinematic properties are also included. The relative yields in the NN bins are taken to be the same as for the signal decays.

A total of 25 parameters are determined from the fit to the $\bar{D}^0\pi^+\pi^-$ sample. These include yields of $B^0 \rightarrow \bar{D}^0\pi^+\pi^-$ decays, the total combinatorial background, the total partially reconstructed background, and the $B_{(s)}^0 \rightarrow \bar{D}^{(*)0}K\pi$ and $A_b^0 \rightarrow D^{(*)0}p\pi^-$ misidentified backgrounds. For $B^0 \rightarrow \bar{D}^0\pi^+\pi^-$ decays, combinatorial and partially reconstructed backgrounds, the fractional yields f_i of each component in bins 1–4 are also free parameters, with the fraction in bin 5 determined as $f_5 = 1 - \sum_{i=1}^4 f_i$. In addition, the exponential slope parameter of the combinatorial background, the fraction of the combinatorial background from $B^+ \rightarrow \bar{D}^{*0}\pi^+$ decays, the fraction of the partially reconstructed background from $B^0 \rightarrow \bar{D}^{*0}\pi^+\pi^-$ decays and the offset parameter of the partially reconstructed background are determined by the fit. Parameters of the signal invariant mass shape (the peak position, the width of the core CB function, and the relative normalisation and ratio of the CB widths) are also allowed to vary. Results of this fit are shown in figure 1.

The fit to the $\bar{D}^0 f_0(980)$ subsample includes the same components as the $B^0 \rightarrow \bar{D}^0\pi^+\pi^-$ fit, with the addition of a second signal component to account for the possible presence of both B^0 and B_s^0 decays. The mass difference between the B^0 and B_s^0 mesons is fixed to the known value [2]. The shapes for the B^0 and B_s^0 components are otherwise identical in both invariant mass and NN output. The following parameters are fixed to the values found in the $B^0 \rightarrow \bar{D}^0\pi^+\pi^-$ fit: the fractional yields f_i for the signal and partially reconstructed background components; the relative normalisation of the two CB functions; the ratio of widths of the CB functions; the fraction of the partially reconstructed background from $B^0 \rightarrow \bar{D}^{*0}\pi^+\pi^-$ decays and the offset parameter of the partially reconstructed background. In addition, the relative yields of the misidentified background components from $B^0 \rightarrow \bar{D}^{(*)0}K^+\pi^-$ and $B_s^0 \rightarrow \bar{D}^{(*)0}K^-\pi^+$ decays are fixed to the expected value [48]. The remaining 14 parameters are: the yields for $B_s^0 \rightarrow \bar{D}^0 f_0(980)$ decays, $B^0 \rightarrow \bar{D}^0\pi^+\pi^-$ decays, combinatorial and partially reconstructed backgrounds and for the $B_{(s)}^0 \rightarrow \bar{D}^{(*)0}K\pi$ and $A_b^0 \rightarrow D^{(*)0}p\pi^-$ misidentified backgrounds; the fractional yields of the combinatorial background in NN output bins, the exponential slope parameter of the combinatorial background and the fraction of the combinatorial background from $B^+ \rightarrow \bar{D}^{*0}\pi^+$ decays; and the signal peak position and core width. Results of this fit are shown in figure 2.

The yields from the fits to the $\bar{D}^0 f_0(980)$ and $\bar{D}^0\pi^+\pi^-$ data samples are summarised in table 1. In total, 29 ± 17 $B_s^0 \rightarrow \bar{D}^0 f_0(980)$ decays are found, with a statistical significance of 2.2σ obtained from $\sqrt{-2 \Delta \ln \mathcal{L}}$, where $\Delta \ln \mathcal{L}$ is the change in log likelihood from the value obtained in a fit with zero signal yield.

5 Systematic uncertainties

The systematic uncertainties that affect the ratio of branching fractions are summarised in table 2. Various effects contribute to the systematic uncertainties on the invariant mass fit and efficiencies, as described below.

The tail parameters of the signal components for $B_s^0 \rightarrow \bar{D}^0 f_0(980)$ and $B^0 \rightarrow \bar{D}^0\pi^+\pi^-$ decays are varied within the uncertainties from the fit to simulated events. For the $B_s^0 \rightarrow \bar{D}^0 f_0(980)$ fit, the relative normalisation and ratio of widths of the CB functions are varied according to the uncertainties from the fit to the $B^0 \rightarrow \bar{D}^0\pi^+\pi^-$ mode. Com-

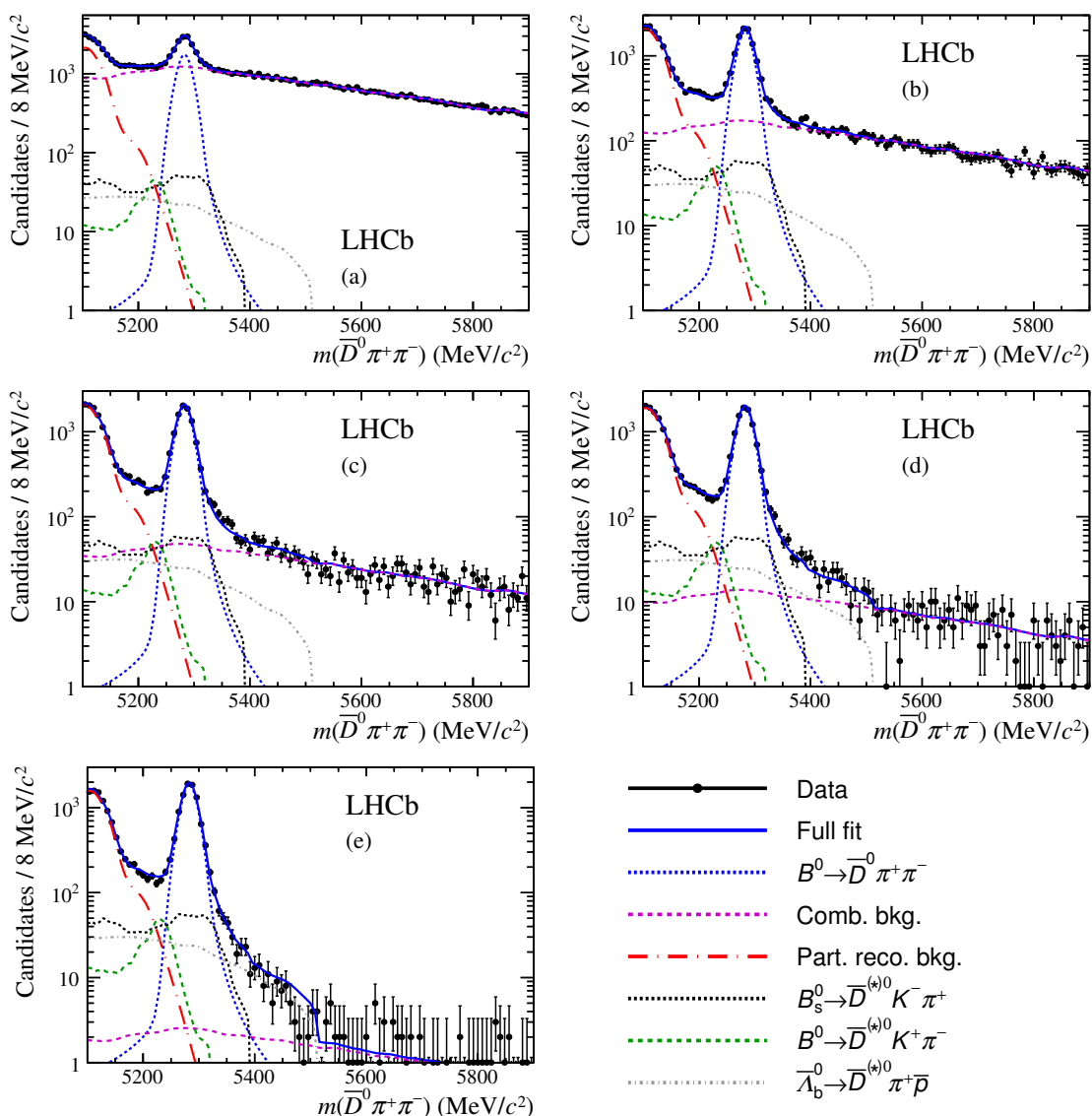


Figure 1. Invariant mass distribution of candidates in the $\bar{D}^0\pi^+\pi^-$ data sample with fit results overlaid, shown on a logarithmic scale. The components are as detailed in the legend. The labels (a) to (e) show the NN bins with increasing purity. The NN binning scheme is described in section 4.

	$\bar{D}^0\pi^+\pi^-$	$\bar{D}^0 f_0(980)$
$B^0 \rightarrow \bar{D}^0\pi^+\pi^-$	$42\,636 \pm 362$	$3\,998 \pm 87$
$B_s^0 \rightarrow \bar{D}^0 f_0(980)$	—	29 ± 17
Combinatorial	$90\,150 \pm 481$	$11\,064 \pm 145$
Partially reconstructed	$50\,950 \pm 493$	$3\,759 \pm 88$
$B_{(s)}^0 \rightarrow \bar{D}^{(*)0} K \pi$	$9\,225 \pm 504$	852 ± 128
$\Lambda_b^0 \rightarrow D^{(*)0} p \pi^-$	$4\,923 \pm 415$	154 ± 135

Table 1. Yields from the fit to the $\bar{D}^0\pi^+\pi^-$ and $\bar{D}^0 f_0(980)$ samples.

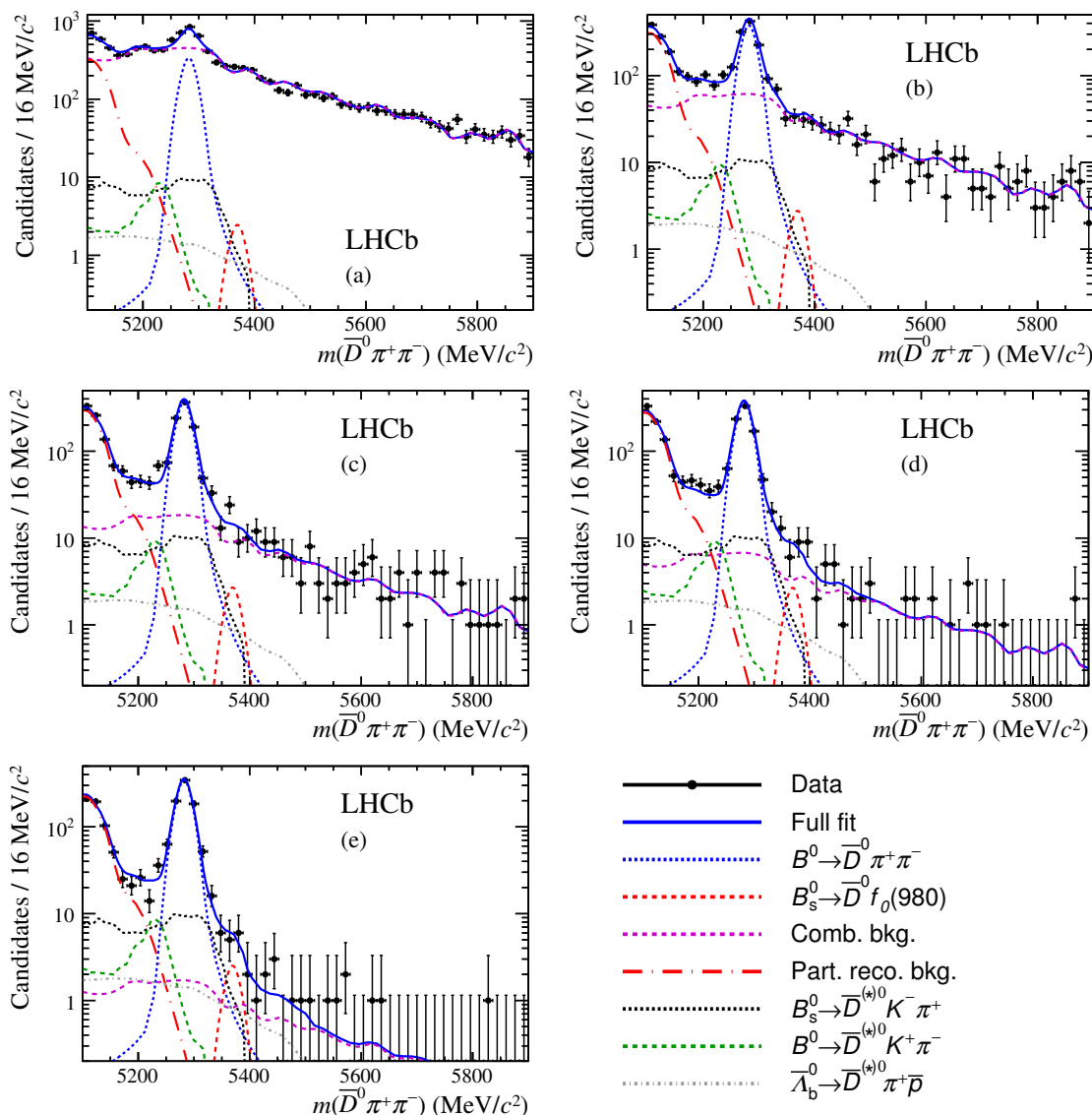


Figure 2. Invariant mass distribution of candidates in the $\bar{D}^0 f_0(980)$ data sample with fit results overlaid, shown on a logarithmic scale. The components are as detailed in the legend. The labels (a) to (e) show the NN bins with increasing purity. The NN binning scheme is described in section 4.

binning in quadrature these contribute 11.5% to the systematic uncertainty. The systematic uncertainty from assuming that the NN response is identical for $B_s^0 \rightarrow \bar{D}^0 f_0(980)$ and $B^0 \rightarrow \bar{D}^0 \pi^+ \pi^-$ decays is evaluated by correcting the fractional yields found in the $B^0 \rightarrow \bar{D}^0 \pi^+ \pi^-$ fit by the ratio of fractional yields found in simulated samples. This contributes 0.3% to the systematic uncertainty.

A second-order polynomial function is used to replace the exponential for the combinatorial background in both fits, giving a systematic uncertainty of 8.4%. Varying the smoothing of the non-parametric shape for $B^+ \rightarrow \bar{D}^{*0} \pi^+$ decays gives the largest source of systematic uncertainty of 23.1%; the size of this effect is determined by that of

the simulated background sample. The fractional yields of the $B^+ \rightarrow \bar{D}^{*0}\pi^+$ component of the combinatorial background are fixed to the values found in simulation, rather than using the same fractional yields as the rest of the combinatorial background. This leads to a systematic uncertainty of 1.0%.

The smoothing of the non-parametric functions for $B^0 \rightarrow \bar{D}^{*0}\pi^+\pi^-$ and $B^+ \rightarrow \bar{D}^0\pi^+\pi^-\pi^+$ is varied in both fits. Additionally, in the $B_s^0 \rightarrow \bar{D}^0 f_0(980)$ sample, the relative normalisation of the shapes is varied within uncertainties from the value found in the $B^0 \rightarrow \bar{D}^0\pi^+\pi^-$ fit. Combined in quadrature these contribute 6.2% to the systematic uncertainty. Allowing the fractional yields of the partially reconstructed background to vary in the $\bar{D}^0 f_0(980)$ fit, instead of being fixed to values found in the $\bar{D}^{*0}\pi^+\pi^-$ fit, contributes 3.1% to the systematic uncertainty.

The misidentified background shapes are also varied by changing the smoothing applied to the non-parametric function. Additionally, the simulation is not reweighted to the known phase-space distributions and the relative normalisation of the $B_{(s)}^0 \rightarrow \bar{D}^{(*)0}K\pi$ shapes is varied within uncertainties. Together these contribute 6.7% to the systematic uncertainty. Corrections, derived from simulation, are applied to the fractional yields for the misidentified backgrounds, which are assumed to behave like signal decays in the default fit. The sum in quadrature of the individual contributions gives a systematic uncertainty of 8.5%.

Potential biases in the fit procedure are investigated using an ensemble of pseudoexperiments. Each of the pseudoexperiments is fitted with the same fit model used to describe the data samples. This study shows that the fit is stable and well behaved and that the associated systematic uncertainty is negligible.

The uncertainty on the ratio of reconstruction and selection efficiencies for the $B_s^0 \rightarrow \bar{D}^0 f_0(980)$ and $B^0 \rightarrow \bar{D}^0\pi^+\pi^-$ final states contributes 2.5% to the systematic uncertainty. This includes statistical uncertainty from the sizes of the simulated samples as well as effects related to the choice of binning in kinematic variables in the evaluation of the PID efficiency and potential differences in the response of the hardware trigger. The simulated sample of $B_s^0 \rightarrow \bar{D}^0 f_0(980)$ decays is generated using a relativistic Breit–Wigner function with a width of 70 MeV for the $f_0(980)$ meson. The true lineshape of the $f_0(980)$ meson can differ from the assumed shape in a process-dependent way, which can affect the fraction of $f_0(980) \rightarrow \pi^+\pi^-$ decays that fall inside the selected $m(\pi^+\pi^-)$ window. No systematic uncertainty is assigned due to this choice of $f_0(980)$ lineshape. Other possible sources of uncertainty on the ratio of efficiencies are negligible.

The limited knowledge of the ratio of fragmentation fractions, $f_s/f_d = 0.259 \pm 0.015$ ([25], f_s/f_d value updated in [26]), contributes 5.8% to the systematic uncertainty. Combining all of the above sources in quadrature, the total systematic uncertainty on the ratio of branching fractions is found to be 30.7%.

6 Results and summary

The relative branching fraction of $B_s^0 \rightarrow \bar{D}^0 f_0(980)$ and $B^0 \rightarrow \bar{D}^0\pi^+\pi^-$ decays is determined by correcting the ratio of yields for the relative efficiencies and fragmentation frac-

Source	Value
Signal shapes	11.5 %
Combinatorial background shapes	24.6 %
Partially reconstructed background shapes	6.9 %
Misidentified background shapes	10.8 %
Efficiencies	2.5 %
Fragmentation fraction f_s/f_d	5.8 %
Total	30.7 %

Table 2. Summary of systematic uncertainties on the ratio of branching fractions.

tions, as shown in eq. (1.1). The total efficiencies are found to be $\epsilon(B_s^0 \rightarrow \bar{D}^0 f_0(980)) = (0.76 \pm 0.02) \%$ and $\epsilon(B^0 \rightarrow \bar{D}^0 \pi^+ \pi^-) = (0.57 \pm 0.02) \%$. These values include contributions from the LHCb detector acceptance and from selection, trigger and PID requirements. The selection and trigger efficiencies are calculated from simulated samples with data-driven corrections applied. The PID efficiency is measured using a control sample of $D^{*-} \rightarrow \bar{D}^0 \pi^-$, $\bar{D}^0 \rightarrow K^+ \pi^-$ decays. Variation of the $B^0 \rightarrow \bar{D}^0 \pi^+ \pi^-$ efficiency over the Dalitz plot is taken into account by weighting the simulation according to the observed Dalitz plot distribution [13].

Using eq. (1.1) the ratio of branching fractions is determined to be

$$\frac{\mathcal{B}(B_s^0 \rightarrow \bar{D}^0 f_0(980))}{\mathcal{B}(B^0 \rightarrow \bar{D}^0 \pi^+ \pi^-)} = (2.0 \pm 1.1 \pm 0.6) \times 10^{-3},$$

where the first uncertainty is statistical and the second systematic. This result is obtained under the assumption that the $B_s^0 \rightarrow \bar{D}^0 \pi^+ \pi^-$ decays proceed uniquely via the $f_0(980)$ resonance within the range $900 \text{ MeV}/c^2 < m(\pi^+ \pi^-) < 1080 \text{ MeV}/c^2$; no systematic uncertainty is assigned due to this assumption. The result can be converted into an absolute branching fraction by multiplying by $\mathcal{B}(B^0 \rightarrow \bar{D}^0 \pi^+ \pi^-) = (8.46 \pm 0.51) \times 10^{-4}$ [13] to give

$$\mathcal{B}(B_s^0 \rightarrow \bar{D}^0 f_0(980)) = (1.7 \pm 1.0 \pm 0.5 \pm 0.1) \times 10^{-6},$$

where the third uncertainty is from $\mathcal{B}(B^0 \rightarrow \bar{D}^0 \pi^+ \pi^-)$. Since the signal yield is not significant, upper limits of

$$\mathcal{B}(B_s^0 \rightarrow \bar{D}^0 f_0(980)) < 3.1 \text{ (3.4)} \times 10^{-6}$$

are set at 90 % (95 %) confidence level. The statistical likelihood curve obtained from the fit is convolved with a Gaussian function of width equal to the systematic uncertainty. The limits obtained are the values within which 90 % (95 %) of the integral of the likelihood in the physical region of non-negative branching fraction are contained.

In summary, a search for the $B_s^0 \rightarrow \bar{D}^0 f_0(980)$ decay has been performed using 3.0 fb^{-1} of pp collision data recorded by the LHCb detector in 2011 and 2012. No significant

	$\mathcal{B}(B^0 \rightarrow \bar{D}^0 f_0)$ [13]	$\mathcal{B}(B_s^0 \rightarrow \bar{D}^0 f_0)$
$f_0(500)$	$(11.2 \pm 0.8 \pm 0.5 \pm 2.1 \pm 0.5) \times 10^{-5}$	—
$f_0(980)$	$(1.34 \pm 0.25 \pm 0.10 \pm 0.46 \pm 0.06) \times 10^{-5}$	$(1.7 \pm 1.0 \pm 0.5 \pm 0.1) \times 10^{-6}$

Table 3. Results for branching fractions for $B_{(s)}^0 \rightarrow \bar{D}^0 f_0(500)$ and $B_{(s)}^0 \rightarrow \bar{D}^0 f_0(980)$ decays. All quoted results correspond to branching fraction for $f_0 \rightarrow \pi^+ \pi^-$ of 100%. There is no experimental result for $\mathcal{B}(B_s^0 \rightarrow \bar{D}^0 f_0(500))$.

signal is observed, and a limit is set on the branching fraction that is below the predicted value [22]. The small yield suggests that much larger data samples will be necessary in order to determine the angle γ of the CKM unitarity triangle with $B_s^0 \rightarrow \bar{D}^0 f_0(980)$ decays. Table 3 shows the current experimental status of measurements of the $B_{(s)}^0 \rightarrow \bar{D}^0 f_0(500)$ and $B_{(s)}^0 \rightarrow \bar{D}^0 f_0(980)$ branching fractions. The pattern of branching fractions is very different to that for the $B_{(s)}^0 \rightarrow J/\psi f_0(500)$ and $B_{(s)}^0 \rightarrow J/\psi f_0(980)$ modes [5–8]. These results may provide insight into the substructure of the scalar mesons.

Acknowledgments

We express our gratitude to our colleagues in the CERN accelerator departments for the excellent performance of the LHC. We thank the technical and administrative staff at the LHCb institutes. We acknowledge support from CERN and from the national agencies: CAPES, CNPq, FAPERJ and FINEP (Brazil); NSFC (China); CNRS/IN2P3 (France); BMBF, DFG, HGF and MPG (Germany); INFN (Italy); FOM and NWO (The Netherlands); MNiSW and NCN (Poland); MEN/IFA (Romania); MinES and FANO (Russia); MinECo (Spain); SNSF and SER (Switzerland); NASU (Ukraine); STFC (United Kingdom); NSF (U.S.A.). The Tier1 computing centres are supported by IN2P3 (France), KIT and BMBF (Germany), INFN (Italy), NWO and SURF (The Netherlands), PIC (Spain), GridPP (United Kingdom). We are indebted to the communities behind the multiple open source software packages on which we depend. We are also thankful for the computing resources and the access to software R&D tools provided by Yandex LLC (Russia). Individual groups or members have received support from EPLANET, Marie Skłodowska-Curie Actions and ERC (European Union), Conseil général de Haute-Savoie, Labex ENIGMASS and OCEVU, Région Auvergne (France), RFBR (Russia), XuntaGal and GENCAT (Spain), Royal Society and Royal Commission for the Exhibition of 1851 (United Kingdom).

Open Access. This article is distributed under the terms of the Creative Commons Attribution License ([CC-BY 4.0](https://creativecommons.org/licenses/by/4.0/)), which permits any use, distribution and reproduction in any medium, provided the original author(s) and source are credited.

References

- [1] C. Amsler et al., *Note on scalar mesons below 2 GeV*, in *Review of particle physics*, *Chin. Phys. C* **38** (2014) 090001.

- [2] PARTICLE DATA GROUP, K.A. Olive et al., *Review of particle physics*, *Chin. Phys. C* **38** (2014) 090001.
- [3] R. Fleischer, R. Kneijens and G. Ricciardi, *Anatomy of $B_{s,d}^0 \rightarrow J/\psi f_0(980)$* , *Eur. Phys. J. C* **71** (2011) 1832 [[arXiv:1109.1112](#)] [[INSPIRE](#)].
- [4] S. Stone and L. Zhang, *Use of $B \rightarrow J/\psi f_0$ decays to discern the $q\bar{q}$ or tetraquark nature of scalar mesons*, *Phys. Rev. Lett.* **111** (2013) 062001 [[arXiv:1305.6554](#)] [[INSPIRE](#)].
- [5] LHCb collaboration, *Analysis of the resonant components in $B_s \rightarrow J/\psi \pi^+ \pi^-$* , *Phys. Rev. D* **86** (2012) 052006 [[arXiv:1204.5643](#)] [[INSPIRE](#)].
- [6] LHCb collaboration, *Analysis of the resonant components in $\bar{B}^0 \rightarrow J/\psi \pi^+ \pi^-$* , *Phys. Rev. D* **87** (2013) 052001 [[arXiv:1301.5347](#)] [[INSPIRE](#)].
- [7] LHCb collaboration, *Measurement of resonant and CP components in $\bar{B}_s^0 \rightarrow J/\psi \pi^+ \pi^-$ decays*, *Phys. Rev. D* **89** (2014) 092006 [[arXiv:1402.6248](#)] [[INSPIRE](#)].
- [8] LHCb collaboration, *Measurement of the resonant and CP components in $\bar{B}^0 \rightarrow J/\psi \pi^+ \pi^-$ decays*, *Phys. Rev. D* **90** (2014) 012003 [[arXiv:1404.5673](#)] [[INSPIRE](#)].
- [9] W.H. Liang and E. Oset, *B^0 and B_s^0 decays into $J/\psi f_0(980)$ and $J/\psi f_0(500)$ and the nature of the scalar resonances*, *Phys. Lett. B* **737** (2014) 70 [[arXiv:1406.7228](#)] [[INSPIRE](#)].
- [10] F.E. Close and A. Kirk, *Interpretation of scalar and axial mesons in LHCb from a historical perspective*, *Phys. Rev. D* **91** (2015) 114015 [[arXiv:1503.06942](#)] [[INSPIRE](#)].
- [11] W.H. Liang, J.-J. Xie and E. Oset, *\bar{B}^0 decay into D^0 and ρ or $f_0(500)$, $f_0(980)$, $a_0(980)$ and \bar{B}_s^0 decay into D^0 and K^{*0} or $\kappa(800)$* , [arXiv:1501.00088](#) [[INSPIRE](#)].
- [12] BELLE collaboration, A. Kuzmin et al., *Study of $\bar{B}^0 \rightarrow D^0 \pi^+ \pi^-$ decays*, *Phys. Rev. D* **76** (2007) 012006 [[hep-ex/0611054](#)] [[INSPIRE](#)].
- [13] LHCb collaboration, *Dalitz plot analysis of $B^0 \rightarrow \bar{D}^0 \pi^+ \pi^-$ decays*, [arXiv:1505.01710](#) [[INSPIRE](#)].
- [14] N. Cabibbo, *Unitary symmetry and leptonic decays*, *Phys. Rev. Lett.* **10** (1963) 531 [[INSPIRE](#)].
- [15] M. Kobayashi and T. Maskawa, *CP violation in the renormalizable theory of weak interaction*, *Prog. Theor. Phys.* **49** (1973) 652 [[INSPIRE](#)].
- [16] M. Gronau and D. London, *How to determine all the angles of the unitarity triangle from $B^0 \rightarrow DK_S^0$ and $B_s^0 \rightarrow D\phi$* , *Phys. Lett. B* **253** (1991) 483 [[INSPIRE](#)].
- [17] M. Gronau, Y. Grossman, N. Shuhmaher, A. Soffer and J. Zupan, *Using untagged $B^0 \rightarrow DK_S$ to determine gamma*, *Phys. Rev. D* **69** (2004) 113003 [[hep-ph/0402055](#)] [[INSPIRE](#)].
- [18] M. Gronau, Y. Grossman, Z. Surujon and J. Zupan, *Enhanced effects on extracting gamma from untagged B^0 and B_s^0 decays*, *Phys. Lett. B* **649** (2007) 61 [[hep-ph/0702011](#)] [[INSPIRE](#)].
- [19] S. Nandi and D. London, *$B_s(\bar{B}_s) \rightarrow D_{CP}^0 K\bar{K}$: detecting and discriminating new physics in B_s - \bar{B}_s mixing*, *Phys. Rev. D* **85** (2012) 114015 [[arXiv:1108.5769](#)] [[INSPIRE](#)].
- [20] W. Wang, *Determining CP-violation angle γ with B decays into a scalar/tensor meson*, *Phys. Rev. D* **85** (2012) 051301 [[arXiv:1110.5194](#)] [[INSPIRE](#)].
- [21] LHCb collaboration, *Observation of the decay $B_s^0 \rightarrow \bar{D}^0 \phi$* , *Phys. Lett. B* **727** (2013) 403 [[arXiv:1308.4583](#)] [[INSPIRE](#)].

- [22] C.S. Kim, R.-H. Li and W. Wang, $B \rightarrow DK_{0,2}^*$ decays: PQCD analysis to determine CP-violation phase angle γ , *Phys. Rev. D* **88** (2013) 034003 [[arXiv:1305.5320](#)] [[INSPIRE](#)].
- [23] LHCb collaboration, First observation of $B_s^0 \rightarrow J/\psi f_0(980)$ decays, *Phys. Lett. B* **698** (2011) 115 [[arXiv:1102.0206](#)] [[INSPIRE](#)].
- [24] LHCb collaboration, Search for the decay $B_s^0 \rightarrow D^{*\mp} \pi^\pm$, *Phys. Rev. D* **87** (2013) 071101 [[arXiv:1302.6446](#)] [[INSPIRE](#)].
- [25] LHCb collaboration, Measurement of the fragmentation fraction ratio f_s/f_d and its dependence on B meson kinematics, *JHEP* **04** (2013) 001 [[arXiv:1301.5286](#)] [[INSPIRE](#)].
- [26] LHCb collaboration, Measurement of the fragmentation fraction ratio f_s/f_d and its dependence on B meson kinematics, LHCb-CONF-2013-011 (2013).
- [27] LHCb collaboration, The LHCb detector at the LHC, 2008 *JINST* **3** S08005 [[INSPIRE](#)].
- [28] LHCb collaboration, LHCb detector performance, *Int. J. Mod. Phys. A* **30** (2015) 1530022 [[arXiv:1412.6352](#)] [[INSPIRE](#)].
- [29] R. Aaij et al., Performance of the LHCb vertex locator, 2014 *JINST* **9** 09007 [[arXiv:1405.7808](#)] [[INSPIRE](#)].
- [30] R. Arink et al., Performance of the LHCb outer tracker, 2014 *JINST* **9** P01002 [[arXiv:1311.3893](#)] [[INSPIRE](#)].
- [31] M. Adinolfi et al., Performance of the LHCb RICH detector at the LHC, *Eur. Phys. J. C* **73** (2013) 2431 [[arXiv:1211.6759](#)] [[INSPIRE](#)].
- [32] A.A. Alves Jr. et al., Performance of the LHCb muon system, 2013 *JINST* **8** P02022 [[arXiv:1211.1346](#)] [[INSPIRE](#)].
- [33] R. Aaij et al., The LHCb trigger and its performance in 2011, 2013 *JINST* **8** P04022 [[arXiv:1211.3055](#)] [[INSPIRE](#)].
- [34] V.V. Gligorov and M. Williams, Efficient, reliable and fast high-level triggering using a bonsai boosted decision tree, 2013 *JINST* **8** P02013 [[arXiv:1210.6861](#)] [[INSPIRE](#)].
- [35] T. Sjöstrand, S. Mrenna and P.Z. Skands, PYTHIA 6.4 physics and manual, *JHEP* **05** (2006) 026 [[hep-ph/0603175](#)] [[INSPIRE](#)].
- [36] T. Sjöstrand, S. Mrenna and P.Z. Skands, A brief introduction to PYTHIA 8.1, *Comput. Phys. Commun.* **178** (2008) 852 [[arXiv:0710.3820](#)] [[INSPIRE](#)].
- [37] I. Belyaev et al., Handling of the generation of primary events in Gauss, the LHCb simulation framework, *J. Phys. Conf. Ser.* **331** (2011) 032047 [[INSPIRE](#)].
- [38] D.J. Lange, The EvtGen particle decay simulation package, *Nucl. Instrum. Meth. A* **462** (2001) 152 [[INSPIRE](#)].
- [39] P. Golonka and Z. Was, PHOTOS Monte Carlo: a precision tool for QED corrections in Z and W decays, *Eur. Phys. J. C* **45** (2006) 97 [[hep-ph/0506026](#)] [[INSPIRE](#)].
- [40] GEANT4 collaboration, J. Allison et al., GEANT4 developments and applications, *IEEE Trans. Nucl. Sci.* **53** (2006) 270.
- [41] GEANT4 collaboration, S. Agostinelli et al., GEANT4 — A Simulation toolkit, *Nucl. Instrum. Meth. A* **506** (2003) 250 [[INSPIRE](#)].
- [42] LHCb collaboration, The LHCb simulation application, Gauss: design, evolution and experience, *J. Phys. Conf. Ser.* **331** (2011) 032023 [[INSPIRE](#)].

- [43] M. Feindt and U. Kerzel, *The NeuroBayes neural network package*, *Nucl. Instrum. Meth. A* **559** (2006) 190 [[INSPIRE](#)].
- [44] M. Pivk and F.R. Le Diberder, *SPlot: a statistical tool to unfold data distributions*, *Nucl. Instrum. Meth. A* **555** (2005) 356 [[physics/0402083](#)] [[INSPIRE](#)].
- [45] LHCb collaboration, *Dalitz plot analysis of $B_s^0 \rightarrow \bar{D}^0 K^- \pi^+$ decays*, *Phys. Rev. D* **90** (2014) 072003 [[arXiv:1407.7712](#)] [[INSPIRE](#)].
- [46] T. Skwarnicki, *A study of the radiative cascade transitions between the Υ' and Υ resonances*, Ph.D. thesis, Institute of Nuclear Physics, Krakow, Poland (1986), [DESY-F31-86-02](#) (1986).
- [47] LHCb collaboration, *First observation and amplitude analysis of the $B^- \rightarrow D^+ K^- \pi^-$ decay*, *Phys. Rev. D* **91** (2015) 092002 [[arXiv:1503.02995](#)] [[INSPIRE](#)].
- [48] LHCb collaboration, *Measurement of the branching fractions of the decays $B_s^0 \rightarrow \bar{D}^0 K^- \pi^+$ and $B^0 \rightarrow \bar{D}^0 K^+ \pi^-$* , *Phys. Rev. D* **87** (2013) 112009 [[arXiv:1304.6317](#)] [[INSPIRE](#)].
- [49] LHCb collaboration, *Studies of beauty baryon decays to $D^0 p h^-$ and $\Lambda_c^+ h^-$ final states*, *Phys. Rev. D* **89** (2014) 032001 [[arXiv:1311.4823](#)] [[INSPIRE](#)].

The LHCb collaboration

R. Aaij³⁸, B. Adeva³⁷, M. Adinolfi⁴⁶, A. Affolder⁵², Z. Ajaltouni⁵, S. Akar⁶, J. Albrecht⁹, F. Alessio³⁸, M. Alexander⁵¹, S. Ali⁴¹, G. Alkhazov³⁰, P. Alvarez Cartelle⁵³, A.A. Alves Jr⁵⁷, S. Amato², S. Amerio²², Y. Amhis⁷, L. An³, L. Anderlini^{17,g}, J. Anderson⁴⁰, M. Andreotti^{16,f}, J.E. Andrews⁵⁸, R.B. Appleby⁵⁴, O. Aquines Gutierrez¹⁰, F. Archilli³⁸, P. d'Argent¹¹, A. Artamonov³⁵, M. Artuso⁵⁹, E. Aslanides⁶, G. Auriemma^{25,n}, M. Baalouch⁵, S. Bachmann¹¹, J.J. Back⁴⁸, A. Badalov³⁶, C. Baesso⁶⁰, W. Baldini^{16,38}, R.J. Barlow⁵⁴, C. Barschel³⁸, S. Barsuk⁷, W. Barter³⁸, V. Batozskaya²⁸, V. Battista³⁹, A. Bay³⁹, L. Beaucourt⁴, J. Beddow⁵¹, F. Bedeschi²³, I. Bediaga¹, L.J. Bel⁴¹, I. Belyaev³¹, E. Ben-Haim⁸, G. Bencivenni¹⁸, S. Benson³⁸, J. Benton⁴⁶, A. Berezhnoy³², R. Bernet⁴⁰, A. Bertolin²², M.-O. Bettler³⁸, M. van Beuzekom⁴¹, A. Bien¹¹, S. Bifani⁴⁵, T. Bird⁵⁴, A. Birnkraut⁹, A. Bizzeti^{17,i}, T. Blake⁴⁸, F. Blanc³⁹, J. Blouw¹⁰, S. Blusk⁵⁹, V. Bocci²⁵, A. Bondar³⁴, N. Bondar^{30,38}, W. Bonivento¹⁵, S. Borghi⁵⁴, M. Borsato⁷, T.J.V. Bowcock⁵², E. Bowen⁴⁰, C. Bozzi¹⁶, S. Braun¹¹, D. Brett⁵⁴, M. Britsch¹⁰, T. Britton⁵⁹, J. Brodzicka⁵⁴, N.H. Brook⁴⁶, A. Bursche⁴⁰, J. Buytaert³⁸, S. Cadeddu¹⁵, R. Calabrese^{16,f}, M. Calvi^{20,k}, M. Calvo Gomez^{36,p}, P. Campana¹⁸, D. Campora Perez³⁸, L. Capriotti⁵⁴, A. Carbone^{14,d}, G. Carboni^{24,l}, R. Cardinale^{19,j}, A. Cardini¹⁵, P. Carniti²⁰, L. Carson⁵⁰, K. Carvalho Akiba^{2,38}, R. Casanova Mohr³⁶, G. Casse⁵², L. Cassina^{20,k}, L. Castillo Garcia³⁸, M. Cattaneo³⁸, Ch. Cauet⁹, G. Cavallero¹⁹, R. Cenci^{23,t}, M. Charles⁸, Ph. Charpentier³⁸, M. Chefdeville⁴, S. Chen⁵⁴, S.-F. Cheung⁵⁵, N. Chiapolini⁴⁰, M. Chrzaszcz^{40,26}, X. Cid Vidal³⁸, G. Ciezarek⁴¹, P.E.L. Clarke⁵⁰, M. Clemencic³⁸, H.V. Cliff⁴⁷, J. Closier³⁸, V. Coco³⁸, J. Cogan⁶, E. Cogneras⁵, V. Cogoni^{15,e}, L. Cojocariu²⁹, G. Collazuol²², P. Collins³⁸, A. Comerma-Montells¹¹, A. Contu^{15,38}, A. Cook⁴⁶, M. Coombes⁴⁶, S. Coquereau⁸, G. Corti³⁸, M. Corvo^{16,f}, B. Couturier³⁸, G.A. Cowan⁵⁰, D.C. Craik⁴⁸, A. Crocombe⁴⁸, M. Cruz Torres⁶⁰, S. Cunliffe⁵³, R. Currie⁵³, C. D'Ambrosio³⁸, J. Dalseno⁴⁶, P.N.Y. David⁴¹, A. Davis⁵⁷, K. De Bruyn⁴¹, S. De Capua⁵⁴, M. De Cian¹¹, J.M. De Miranda¹, L. De Paula², W. De Silva⁵⁷, P. De Simone¹⁸, C.-T. Dean⁵¹, D. Decamp⁴, M. Deckenhoff⁹, L. Del Buono⁸, N. Déléage⁴, D. Derkach⁵⁵, O. Deschamps⁵, F. Dettori³⁸, B. Dey⁴⁰, A. Di Canto³⁸, F. Di Ruscio²⁴, H. Dijkstra³⁸, S. Donleavy⁵², F. Dordei¹¹, M. Dorigo³⁹, A. Dosil Suárez³⁷, D. Dossett⁴⁸, A. Dovbnya⁴³, K. Dreimanic⁵², G. Dujany⁵⁴, F. Dupertuis³⁹, P. Durante³⁸, R. Dzhelyadin³⁵, A. Dziurda²⁶, A. Dzyuba³⁰, S. Easo^{49,38}, U. Egede⁵³, V. Egorychev³¹, S. Eidelman³⁴, S. Eisenhardt⁵⁰, U. Eitschberger⁹, R. Ekelhof⁹, L. Eklund⁵¹, I. El Rifai⁵, Ch. Elsasser⁴⁰, S. Ely⁵⁹, S. Esen¹¹, H.M. Evans⁴⁷, T. Evans⁵⁵, A. Falabella¹⁴, C. Färber¹¹, C. Farinelli⁴¹, N. Farley⁴⁵, S. Farry⁵², R. Fay⁵², D. Ferguson⁵⁰, V. Fernandez Albor³⁷, F. Ferrari¹⁴, F. Ferreira Rodrigues¹, M. Ferro-Luzzi³⁸, S. Filippov³³, M. Fiore^{16,38,f}, M. Fiorini^{16,f}, M. Firlej²⁷, C. Fitzpatrick³⁹, T. Fiutowski²⁷, P. Fol⁵³, M. Fontana¹⁰, F. Fontanelli^{19,j}, R. Forty³⁸, O. Francisco², M. Frank³⁸, C. Frei³⁸, M. Frosini¹⁷, J. Fu²¹, E. Furfaro^{24,l}, A. Gallas Torreira³⁷, D. Galli^{14,d}, S. Gallorini^{22,38}, S. Gambetta^{19,j}, M. Gandelman², P. Gandini⁵⁵, Y. Gao³, J. García Pardiñas³⁷, J. Garofoli⁵⁹, J. Garra Tico⁴⁷, L. Garrido³⁶, D. Gascon³⁶, C. Gaspar³⁸, U. Gastaldi¹⁶, R. Gauld⁵⁵, L. Gavardi⁹, G. Gazzoni⁵, A. Geraci^{21,v}, D. Gerick¹¹, E. Gersabeck¹¹, M. Gersabeck⁵⁴, T. Gershon⁴⁸, Ph. Ghez⁴, A. Gianelle²², S. Gianì³⁹, V. Gibson⁴⁷, L. Giubega²⁹, V.V. Gligorov³⁸, C. Göbel⁶⁰, D. Golubkov³¹, A. Golutvin^{53,31,38}, A. Gomes^{1,a}, C. Gotti^{20,k}, M. Grabalosa Gándara⁵, R. Graciani Diaz³⁶, L.A. Granado Cardoso³⁸, E. Graugés³⁶, E. Graverini⁴⁰, G. Graziani¹⁷, A. Grecu²⁹, E. Greening⁵⁵, S. Gregson⁴⁷, P. Griffith⁴⁵, L. Grillo¹¹, O. Grünberg⁶³, B. Gui⁵⁹, E. Gushchin³³, Yu. Guz^{35,38}, T. Gys³⁸, C. Hadjivasiliou⁵⁹, G. Haefeli³⁹, C. Haen³⁸, S.C. Haines⁴⁷, S. Hall⁵³, B. Hamilton⁵⁸, T. Hampson⁴⁶, X. Han¹¹, S. Hansmann-Menzemer¹¹, N. Harnew⁵⁵, S.T. Harnew⁴⁶, J. Harrison⁵⁴, J. He³⁸, T. Head³⁹, V. Heijne⁴¹, K. Hennessy⁵², P. Henrard⁵, L. Henry⁸, J.A. Hernando Morata³⁷, E. van Herwijnen³⁸, M. Heß⁶³, A. Hicheur², D. Hill⁵⁵,

M. Hoballah⁵, C. Hombach⁵⁴, W. Hulsbergen⁴¹, T. Humair⁵³, N. Hussain⁵⁵, D. Hutchcroft⁵²,
 D. Hynds⁵¹, M. Idzik²⁷, P. Ilten⁵⁶, R. Jacobsson³⁸, A. Jaeger¹¹, J. Jalocha⁵⁵, E. Jans⁴¹,
 A. Jawahery⁵⁸, F. Jing³, M. John⁵⁵, D. Johnson³⁸, C.R. Jones⁴⁷, C. Joram³⁸, B. Jost³⁸,
 N. Jurik⁵⁹, S. Kandybei⁴³, W. Kanso⁶, M. Karacson³⁸, T.M. Karbach^{38,†}, S. Karodia⁵¹,
 M. Kelsey⁵⁹, I.R. Kenyon⁴⁵, M. Kenzie³⁸, T. Ketel⁴², B. Khanji^{20,38,k}, C. Khurewathanakul³⁹,
 S. Klaver⁵⁴, K. Klimaszewski²⁸, O. Kochebina⁷, M. Kolpin¹¹, I. Komarov³⁹, R.F. Koopman⁴²,
 P. Koppenburg^{41,38}, M. Korolev³², L. Kravchuk³³, K. Kreplin¹¹, M. Kreps⁴⁸, G. Krocker¹¹,
 P. Krokovny³⁴, F. Kruse⁹, W. Kucewicz^{26,o}, M. Kucharczyk²⁶, V. Kudryavtsev³⁴, K. Kurek²⁸,
 T. Kvaratskheliya³¹, V.N. La Thi³⁹, D. Lacarrere³⁸, G. Lafferty⁵⁴, A. Lai¹⁵, D. Lambert⁵⁰,
 R.W. Lambert⁴², G. Lanfranchi¹⁸, C. Langenbruch⁴⁸, B. Langhans³⁸, T. Latham⁴⁸,
 C. Lazzeroni⁴⁵, R. Le Gac⁶, J. van Leerdam⁴¹, J.-P. Lees⁴, R. Lefèvre⁵, A. Leflat³², J. Lefrançois⁷,
 O. Leroy⁶, T. Lesiak²⁶, B. Leverington¹¹, Y. Li⁷, T. Likhomanenko^{65,64}, M. Liles⁵², R. Lindner³⁸,
 C. Linn³⁸, F. Lionetto⁴⁰, B. Liu¹⁵, S. Lohn³⁸, I. Longstaff⁵¹, J.H. Lopes², D. Lucchesi^{22,r},
 M. Lucio Martinez³⁷, H. Luo⁵⁰, A. Lupato²², E. Luppi^{16,f}, O. Lupton⁵⁵, F. Machefert⁷,
 F. Maciuc²⁹, O. Maev³⁰, S. Malde⁵⁵, A. Malinin⁶⁴, G. Manca^{15,e}, G. Mancinelli⁶, P. Manning⁵⁹,
 A. Mapelli³⁸, J. Maratas⁵, J.F. Marchand⁴, U. Marconi¹⁴, C. Marin Benito³⁶, P. Marino^{23,38,t},
 R. Märki³⁹, J. Marks¹¹, G. Martellotti²⁵, M. Martinelli³⁹, D. Martinez Santos⁴²,
 F. Martinez Vidal⁶⁶, D. Martins Tostes², A. Massafferri¹, R. Matev³⁸, A. Mathad⁴⁸, Z. Mathe³⁸,
 C. Matteuzzi²⁰, K. Matthieu¹¹, A. Mauri⁴⁰, B. Maurin³⁹, A. Mazurov⁴⁵, M. McCann⁵³,
 J. McCarthy⁴⁵, A. McNab⁵⁴, R. McNulty¹², B. Meadows⁵⁷, F. Meier⁹, M. Meissner¹¹, M. Merk⁴¹,
 D.A. Milanes⁶², M.-N. Minard⁴, D.S. Mitzel¹¹, J. Molina Rodriguez⁶⁰, S. Monteil⁵,
 M. Morandin²², P. Morawski²⁷, A. Mordà⁶, M.J. Morello^{23,t}, J. Moron²⁷, A.B. Morris⁵⁰,
 R. Mountain⁵⁹, F. Muheim⁵⁰, J. Müller⁹, K. Müller⁴⁰, V. Müller⁹, M. Mussini¹⁴, B. Muster³⁹,
 P. Naik⁴⁶, T. Nakada³⁹, R. Nandakumar⁴⁹, I. Nasteva², M. Needham⁵⁰, N. Neri²¹, S. Neubert¹¹,
 N. Neufeld³⁸, M. Neuner¹¹, A.D. Nguyen³⁹, T.D. Nguyen³⁹, C. Nguyen-Mau^{39,q}, V. Niess⁵,
 R. Niet⁹, N. Nikitin³², T. Nikodem¹¹, D. Ninci²³, A. Novoselov³⁵, D.P. O’Hanlon⁴⁸,
 A. Oblakowska-Mucha²⁷, V. Obraztsov³⁵, S. Ogilvy⁵¹, O. Okhrimenko⁴⁴, R. Oldeman^{15,e},
 C.J.G. Onderwater⁶⁷, B. Osorio Rodrigues¹, J.M. Otalora Goicochea², A. Otto³⁸, P. Owen⁵³,
 A. Oyanguren⁶⁶, A. Palano^{13,c}, F. Palombo^{21,u}, M. Palutan¹⁸, J. Panman³⁸, A. Papanestis⁴⁹,
 M. Pappagallo⁵¹, L.L. Pappalardo^{16,f}, C. Parkes⁵⁴, G. Passaleva¹⁷, G.D. Patel⁵², M. Patel⁵³,
 C. Patrignani^{19,j}, A. Pearce^{54,49}, A. Pellegrino⁴¹, G. Penso^{25,m}, M. Pepe Altarelli³⁸,
 S. Perazzini^{14,d}, P. Perret⁵, L. Pescatore⁴⁵, K. Petridis⁴⁶, A. Petrolini^{19,j}, M. Petruzzo²¹,
 E. Picatoste Olloqui³⁶, B. Pietrzyk⁴, T. Pilar⁴⁸, D. Pinci²⁵, A. Pistone¹⁹, S. Playfer⁵⁰,
 M. Plo Casasus³⁷, T. Poikela³⁸, F. Polci⁸, A. Poluektov^{48,34}, I. Polyakov³¹, E. Polcarpo²,
 A. Popov³⁵, D. Popov¹⁰, B. Popovici²⁹, C. Potterat², E. Price⁴⁶, J.D. Price⁵², J. Prisciandaro³⁹,
 A. Pritchard⁵², C. Prouve⁴⁶, V. Pugatch⁴⁴, A. Puig Navarro³⁹, G. Punzi^{23,s}, W. Qian⁴,
 R. Quagliani^{7,46}, B. Rachwal²⁶, J.H. Rademacker⁴⁶, B. Rakotomiamanana³⁹, M. Rama²³,
 M.S. Rangel², I. Raniuk⁴³, N. Rauschmayr³⁸, G. Raven⁴², F. Redi⁵³, S. Reichert⁵⁴, M.M. Reid⁴⁸,
 A.C. dos Reis¹, S. Ricciardi⁴⁹, S. Richards⁴⁶, M. Rihl³⁸, K. Rinnert⁵², V. Rives Molina³⁶,
 P. Robbe^{7,38}, A.B. Rodrigues¹, E. Rodrigues⁵⁴, J.A. Rodriguez Lopez⁶², P. Rodriguez Perez⁵⁴,
 S. Roiser³⁸, V. Romanovsky³⁵, A. Romero Vidal³⁷, M. Rotondo²², J. Rouvinet³⁹, T. Ruf³⁸,
 H. Ruiz³⁶, P. Ruiz Valls⁶⁶, J.J. Saborido Silva³⁷, N. Sagidova³⁰, P. Sail⁵¹, B. Saitta^{15,e},
 V. Salustino Guimaraes², C. Sanchez Mayordomo⁶⁶, B. Sanmartin Sedes³⁷, R. Santacesaria²⁵,
 C. Santamarina Rios³⁷, E. Santovetti^{24,l}, A. Sarti^{18,m}, C. Satriano^{25,n}, A. Satta²⁴,
 D.M. Saunders⁴⁶, D. Savrina^{31,32}, M. Schiller³⁸, H. Schindler³⁸, M. Schlupp⁹, M. Schmelling¹⁰,
 T. Schmelzer⁹, B. Schmidt³⁸, O. Schneider³⁹, A. Schopper³⁸, M.-H. Schune⁷, R. Schwemmer³⁸,
 B. Sciascia¹⁸, A. Sciubba^{25,m}, A. Semennikov³¹, I. Sepp⁵³, N. Serra⁴⁰, J. Serrano⁶, L. Sestini²²,
 P. Seyfert¹¹, M. Shapkin³⁵, I. Shapoval^{16,43,f}, Y. Shcheglov³⁰, T. Shears⁵², L. Shekhtman³⁴,

V. Shevchenko⁶⁴, A. Shires⁹, R. Silva Coutinho⁴⁸, G. Simi²², M. Sirendi⁴⁷, N. Skidmore⁴⁶, I. Skillicorn⁵¹, T. Skwarnicki⁵⁹, E. Smith^{55,49}, E. Smith⁵³, J. Smith⁴⁷, M. Smith⁵⁴, H. Snoek⁴¹, M.D. Sokoloff^{57,38}, F.J.P. Soler⁵¹, F. Soomro³⁹, D. Souza⁴⁶, B. Souza De Paula², B. Spaan⁹, P. Spradlin⁵¹, S. Sridharan³⁸, F. Stagni³⁸, M. Stahl¹¹, S. Stahl³⁸, O. Steinkamp⁴⁰, O. Stenyakin³⁵, F. Sterpka⁵⁹, S. Stevenson⁵⁵, S. Stoica²⁹, S. Stone⁵⁹, B. Storaci⁴⁰, S. Stracka^{23,t}, M. Straticiu²⁹, U. Straumann⁴⁰, R. Stroili²², L. Sun⁵⁷, W. Sutcliffe⁵³, K. Swientek²⁷, S. Swientek⁹, V. Syropoulos⁴², M. Szczekowski²⁸, P. Szczypka^{39,38}, T. Szumlak²⁷, S. T'Jampens⁴, T. Tekampe⁹, M. Teklishyn⁷, G. Tellarini^{16,f}, F. Teubert³⁸, C. Thomas⁵⁵, E. Thomas³⁸, J. van Tilburg⁴¹, V. Tisserand⁴, M. Tobin³⁹, J. Todd⁵⁷, S. Tolk⁴², L. Tomassetti^{16,f}, D. Tonelli³⁸, S. Topp-Joergensen⁵⁵, N. Torr⁵⁵, E. Tournefier⁴, S. Tourneur³⁹, K. Trabelsi³⁹, M.T. Tran³⁹, M. Tresch⁴⁰, A. Trisovic³⁸, A. Tsaregorodtsev⁶, P. Tsopelas⁴¹, N. Tuning^{41,38}, A. Ukleja²⁸, A. Ustyuzhanin^{65,64}, U. Uwer¹¹, C. Vacca^{15,e}, V. Vagnoni¹⁴, G. Valenti¹⁴, A. Vallier⁷, R. Vazquez Gomez¹⁸, P. Vazquez Regueiro³⁷, C. Vázquez Sierra³⁷, S. Vecchi¹⁶, J.J. Velthuis⁴⁶, M. Veltri^{17,h}, G. Veneziano³⁹, M. Vesterinen¹¹, B. Viaud⁷, D. Vieira², M. Vieites Diaz³⁷, X. Vilasis-Cardona^{36,p}, A. Vollhardt⁴⁰, D. Volyansky¹⁰, D. Voong⁴⁶, A. Vorobyev³⁰, V. Vorobyev³⁴, C. Vob⁶³, J.A. de Vries⁴¹, R. Waldi⁶³, C. Wallace⁴⁸, R. Wallace¹², J. Walsh²³, S. Wandernoth¹¹, J. Wang⁵⁹, D.R. Ward⁴⁷, N.K. Watson⁴⁵, D. Websdale⁵³, A. Weiden⁴⁰, M. Whitehead⁴⁸, D. Wiedner¹¹, G. Wilkinson^{55,38}, M. Wilkinson⁵⁹, M. Williams³⁸, M.P. Williams⁴⁵, M. Williams⁵⁶, F.F. Wilson⁴⁹, J. Wimberley⁵⁸, J. Wishahi⁹, W. Wislicki²⁸, M. Witek²⁶, G. Wormser⁷, S.A. Wotton⁴⁷, S. Wright⁴⁷, K. Wyllie³⁸, Y. Xie⁶¹, Z. Xu³⁹, Z. Yang³, X. Yuan³⁴, O. Yushchenko³⁵, M. Zangoli¹⁴, M. Zavertyaev^{10,b}, L. Zhang³, Y. Zhang³, A. Zhelezov¹¹, A. Zhokhov³¹, L. Zhong³

¹ Centro Brasileiro de Pesquisas Físicas (CBPF), Rio de Janeiro, Brazil

² Universidade Federal do Rio de Janeiro (UFRJ), Rio de Janeiro, Brazil

³ Center for High Energy Physics, Tsinghua University, Beijing, China

⁴ LAPP, Université Savoie Mont-Blanc, CNRS/IN2P3, Annecy-Le-Vieux, France

⁵ Clermont Université, Université Blaise Pascal, CNRS/IN2P3, LPC, Clermont-Ferrand, France

⁶ CPPM, Aix-Marseille Université, CNRS/IN2P3, Marseille, France

⁷ LAL, Université Paris-Sud, CNRS/IN2P3, Orsay, France

⁸ LPNHE, Université Pierre et Marie Curie, Université Paris Diderot, CNRS/IN2P3, Paris, France

⁹ Fakultät Physik, Technische Universität Dortmund, Dortmund, Germany

¹⁰ Max-Planck-Institut für Kernphysik (MPIK), Heidelberg, Germany

¹¹ Physikalisches Institut, Ruprecht-Karls-Universität Heidelberg, Heidelberg, Germany

¹² School of Physics, University College Dublin, Dublin, Ireland

¹³ Sezione INFN di Bari, Bari, Italy

¹⁴ Sezione INFN di Bologna, Bologna, Italy

¹⁵ Sezione INFN di Cagliari, Cagliari, Italy

¹⁶ Sezione INFN di Ferrara, Ferrara, Italy

¹⁷ Sezione INFN di Firenze, Firenze, Italy

¹⁸ Laboratori Nazionali dell'INFN di Frascati, Frascati, Italy

¹⁹ Sezione INFN di Genova, Genova, Italy

²⁰ Sezione INFN di Milano Bicocca, Milano, Italy

²¹ Sezione INFN di Milano, Milano, Italy

²² Sezione INFN di Padova, Padova, Italy

²³ Sezione INFN di Pisa, Pisa, Italy

²⁴ Sezione INFN di Roma Tor Vergata, Roma, Italy

²⁵ Sezione INFN di Roma La Sapienza, Roma, Italy

²⁶ Henryk Niewodniczanski Institute of Nuclear Physics Polish Academy of Sciences, Kraków, Poland

²⁷ AGH - University of Science and Technology, Faculty of Physics and Applied Computer Science, Kraków, Poland

- ²⁸ *National Center for Nuclear Research (NCBJ), Warsaw, Poland*
- ²⁹ *Horia Hulubei National Institute of Physics and Nuclear Engineering, Bucharest-Magurele, Romania*
- ³⁰ *Petersburg Nuclear Physics Institute (PNPI), Gatchina, Russia*
- ³¹ *Institute of Theoretical and Experimental Physics (ITEP), Moscow, Russia*
- ³² *Institute of Nuclear Physics, Moscow State University (SINP MSU), Moscow, Russia*
- ³³ *Institute for Nuclear Research of the Russian Academy of Sciences (INR RAN), Moscow, Russia*
- ³⁴ *Budker Institute of Nuclear Physics (SB RAS) and Novosibirsk State University, Novosibirsk, Russia*
- ³⁵ *Institute for High Energy Physics (IHEP), Protvino, Russia*
- ³⁶ *Universitat de Barcelona, Barcelona, Spain*
- ³⁷ *Universidad de Santiago de Compostela, Santiago de Compostela, Spain*
- ³⁸ *European Organization for Nuclear Research (CERN), Geneva, Switzerland*
- ³⁹ *Ecole Polytechnique Fédérale de Lausanne (EPFL), Lausanne, Switzerland*
- ⁴⁰ *Physik-Institut, Universität Zürich, Zürich, Switzerland*
- ⁴¹ *Nikhef National Institute for Subatomic Physics, Amsterdam, The Netherlands*
- ⁴² *Nikhef National Institute for Subatomic Physics and VU University Amsterdam, Amsterdam, The Netherlands*
- ⁴³ *NSC Kharkiv Institute of Physics and Technology (NSC KIPT), Kharkiv, Ukraine*
- ⁴⁴ *Institute for Nuclear Research of the National Academy of Sciences (KINR), Kyiv, Ukraine*
- ⁴⁵ *University of Birmingham, Birmingham, United Kingdom*
- ⁴⁶ *H.H. Wills Physics Laboratory, University of Bristol, Bristol, United Kingdom*
- ⁴⁷ *Cavendish Laboratory, University of Cambridge, Cambridge, United Kingdom*
- ⁴⁸ *Department of Physics, University of Warwick, Coventry, United Kingdom*
- ⁴⁹ *STFC Rutherford Appleton Laboratory, Didcot, United Kingdom*
- ⁵⁰ *School of Physics and Astronomy, University of Edinburgh, Edinburgh, United Kingdom*
- ⁵¹ *School of Physics and Astronomy, University of Glasgow, Glasgow, United Kingdom*
- ⁵² *Oliver Lodge Laboratory, University of Liverpool, Liverpool, United Kingdom*
- ⁵³ *Imperial College London, London, United Kingdom*
- ⁵⁴ *School of Physics and Astronomy, University of Manchester, Manchester, United Kingdom*
- ⁵⁵ *Department of Physics, University of Oxford, Oxford, United Kingdom*
- ⁵⁶ *Massachusetts Institute of Technology, Cambridge, MA, United States*
- ⁵⁷ *University of Cincinnati, Cincinnati, OH, United States*
- ⁵⁸ *University of Maryland, College Park, MD, United States*
- ⁵⁹ *Syracuse University, Syracuse, NY, United States*
- ⁶⁰ *Pontifícia Universidade Católica do Rio de Janeiro (PUC-Rio), Rio de Janeiro, Brazil, associated to²*
- ⁶¹ *Institute of Particle Physics, Central China Normal University, Wuhan, Hubei, China, associated to³*
- ⁶² *Departamento de Física , Universidad Nacional de Colombia, Bogota, Colombia, associated to⁸*
- ⁶³ *Institut für Physik, Universität Rostock, Rostock, Germany, associated to¹¹*
- ⁶⁴ *National Research Centre Kurchatov Institute, Moscow, Russia, associated to³¹*
- ⁶⁵ *Yandex School of Data Analysis, Moscow, Russia, associated to³¹*
- ⁶⁶ *Instituto de Física Corpuscular (IFIC), Universitat de Valencia-CSIC, Valencia, Spain, associated to³⁶*
- ⁶⁷ *Van Swinderen Institute, University of Groningen, Groningen, The Netherlands, associated to⁴¹*
- ^a *Universidade Federal do Triângulo Mineiro (UFTM), Uberaba-MG, Brazil*
- ^b *P.N. Lebedev Physical Institute, Russian Academy of Science (LPI RAS), Moscow, Russia*
- ^c *Università di Bari, Bari, Italy*
- ^d *Università di Bologna, Bologna, Italy*
- ^e *Università di Cagliari, Cagliari, Italy*

- ^f *Università di Ferrara, Ferrara, Italy*
- ^g *Università di Firenze, Firenze, Italy*
- ^h *Università di Urbino, Urbino, Italy*
- ⁱ *Università di Modena e Reggio Emilia, Modena, Italy*
- ^j *Università di Genova, Genova, Italy*
- ^k *Università di Milano Bicocca, Milano, Italy*
- ^l *Università di Roma Tor Vergata, Roma, Italy*
- ^m *Università di Roma La Sapienza, Roma, Italy*
- ⁿ *Università della Basilicata, Potenza, Italy*
- ^o *AGH - University of Science and Technology, Faculty of Computer Science, Electronics and Telecommunications, Kraków, Poland*
- ^p *LIFAELS, La Salle, Universitat Ramon Llull, Barcelona, Spain*
- ^q *Hanoi University of Science, Hanoi, Viet Nam*
- ^r *Università di Padova, Padova, Italy*
- ^s *Università di Pisa, Pisa, Italy*
- ^t *Scuola Normale Superiore, Pisa, Italy*
- ^u *Università degli Studi di Milano, Milano, Italy*
- ^v *Politecnico di Milano, Milano, Italy*
- [†] *Deceased*